HHS Public Access

Author manuscript

Nat Med. Author manuscript; available in PMC 2015 February 01.

Published in final edited form as:

Nat Med. 2014 August ; 20(8): 911–918. doi:10.1038/nm.3615.

Notch signaling regulates adipose browning and energy metabolism

Pengpeng Bi[1], **Tizhong Shan**[1], **Weiyi Liu**[1], **Feng Yue**[1], **Xin Yang**[1], **Xin-Rong Liang**[1], **Jinghua Wang**[1], **Jie Li**[2], **Nadia Carlesso**[3], **Xiaoqi Liu**[2,4], and **Shihuan Kuang**[1,4,*]

[1]Department of Animal Sciences, Purdue University, West Lafayette, IN 47907, USA.

[2]Department of Biochemistry, Purdue University, West Lafayette, IN 47907, USA.

[3]Department of Pediatrics, Indiana University School of Medicine, Indianapolis, IN 46202, USA.

[4]Center for Cancer Research, Purdue University, West Lafayette, IN 47907, USA.

Beige adipocytes in white adipose tissues (WAT) are similar to classical brown adipocytes in that they can burn lipid storage to produce heat. Thus, an increase in beige adipocyte content (browning) in WAT would raise energy expenditure and reduce adiposity. Here we report that adipose-specific inactivation of *Notch1* or its signaling mediator *Rbpj* in mice results in browning of WAT and elevated expression of UCP1, a key regulator of thermogenesis. Consequently, Notch mutants exhibit elevated energy expenditure, better glucose tolerance, improved insulin sensitivity, and are more resistant to high fat diet (HFD)-induced obesity. By contrast, adipose-specific activation of Notch1 leads to opposite phenotypes. At the molecular level, constitutive activation of Notch signaling inhibits, whereas Notch inhibition induces, *Ppargc1a* and *Prdm16* transcription in white adipocytes. Notably, pharmacological inhibition of Notch signaling in obese mice ameliorates obesity, reduces blood glucose and increases UCP1 expression in white fat. Therefore, Notch signaling may be therapeutically targeted to treat obesity and Type 2 diabetes (T2D).

Global epidemics of obesity and its associated risks of chronic diseases including T2D pose formidable challenges to human health. Classical brown adipose tissues (BAT) prominently found in rodents and hibernating mammals dissipate extra energy to generate heat through uncoupled respiration mediated by UCP1, and thus increase energy expenditure and counteract obesity[1-4]. Metabolically active UCP1^{+} brown adipocytes have recently been detected in adult humans with advanced imaging techniques[5-9]. Interestingly, human adipose depots are highly heterogeneous and the brown adipocytes coexist with white and beige (brite) adipocytes[10-12]. Beige adipocytes are a class of adaptive thermogenic cells located within various depots of WAT[13-17]. Recent studies indicate that beige adipocyte homeostasis can be maintained through two mechanisms. First, they can be generated *de*

*Correspondence:skuang@purdue.edu.

AUTHOR CONTRIBUTIONS PB and SK conceived the project, designed the experiments and prepared the manuscript. PB, TS, WL, FY, XY, XRL, JW, JL performed the experiments. NC provided reagents. PB, TS, WL, XL, SK analyzed the data.

COMPETING FINANCIAL INTERESTS The authors declare no competing financial interests.

novo from a population of beige preadipocytes[18,19]. Second, they can be bidirectionally converted from and to white adipocytes under the control of environmental temperature or sympathetic nerve innervation[20-22]. Importantly, elevated UCP1 expression in cold acclimated beige adipocytes is associated with robust uncoupled respiration and thermogenesis[23]. Notably, appearance of beige or brown adipocytes in human is inversely correlated with obesity and T2D mellitus[24,25], indicating their important role in regulating metabolism. Thus, identifying mechanisms underlying beige adipocyte biogenesis is instrumental to the development of therapeutics to reduce adiposity and risks of obesity-related metabolic syndrome that affect over 10% of the world population.

Notch signaling is activated by binding of Dll or Jag family ligands with Notch receptors (Notch1–4), leading to γ-secretase mediated proteolytic cleavage and release of Notch intracellular domain (NICD)[26]. NICD then translocates to the nucleus where it binds with the Rbpj transcriptional complex to activate the transcription of downstream targets, including Hes and Hey family genes. Notch signaling has been shown to paradoxically either inhibit or facilitate the adipogenic differentiation of 3T3 L1 cells[27-30]. In murine and human primary cell cultures, Notch inhibition promotes, while Notch activation inhibits, adipogenic differentiation of mesenchymal and adipose-derived stem cells[31-33]. However, genetic ablation of several key components of the signaling pathway indicates that Notch signaling is dispensable for adipogenesis of mouse embryonic stem cells or embryonic fibroblasts derived from early embryos[34]. As these studies are conducted in cultured cells, the function of Notch signaling in adipose tissues *in vivo* remains unknown.

RESULTS

White to brown fat transition in adipose-specific Notch mutant mice

We first examined the relative expression of Notch pathway genes in different depots of WAT. Notably, the mRNA levels of *Notch* receptors and Notch targets were much higher in visceral epididymal (Epi) WAT than in subcutaneous inguinal (Ing) WAT (Supplementary Fig. 1a,b). By contrast, BAT-specific *Ucp1*, *Ppargc1a* and *Prdm16* were expressed at lower levels in EpiWAT than in IngWAT (Supplementary Fig. 1c). An inverse correlation between activated Notch1 (N1ICD) and UCP1 at the protein level was also observed (Supplementary Fig. 1d). These results suggest that Notch signaling may play a role in regulating BAT-specific gene expression *in vivo*.

To directly investigate how Notch signaling regulates adipose plasticity *in vivo*, we established an adipose-specific *Notch1* knockout mouse model: *aP2-Cre/Notch1*$^{flox/flox}$, henceforth named as *aNotch1*. To validate the tissue specificity of *aP2-Cre*, we evaluated YFP fluorescence in different organs of *aP2-Cre/Rosa*^{EYFP} reporter mice. As expected, adipocytes were all YFP^{+}, but liver and muscle tissues, two important regulators of lipid and glucose homeostasis, were predominately YFP^{-} with only few YFP^{+} interstitial cells (Supplementary Fig. 2a). Adipose macrophages, accounting for < 2% of total stromal vascular fraction (SVF) cells, were also predominantly YFP^{-} (Supplementary Fig. 2b,c). PCR-based genotyping confirmed DNA recombination in adipose tissues of *aNotch1* mice (Supplementary Fig. 2d). Accordingly, *Notch1* expression was ~ 65% lower in adipose tissues and 85% lower in mature adipocytes, but unchanged in other tissues of the *aNotch1*

mice when compared to the wild-type (WT) mice (Supplementary Fig. 2e). Notably, various depots of subcutaneous WAT of *aNotch1* mice appeared browner than their WT counterparts (Fig. 1a). In addition, the weight of various fat depots was lighter in the *aNotch1* compared to WT mice (Fig. 1b). Furthermore, multilocular UCP1^{+} beige adipocytes were much more abundant in the IngWAT of *aNotch1* versus in WT mice (Fig. 1c). The average adipocyte sizes of *aNotch1* WAT were ~ 40% smaller than those of WT (Fig. 1c). At the molecular level, expression of *Ucp1*, *Cidea*, *Prdm16*, *Ppargc1a* genes were upregulated in the IngWAT of *aNotch1* mice compared with WT mice (Fig. 1d). Western blot confirmed the higher UCP1 protein levels in the *aNotch1* IngWAT (Fig. 1e). In addition, mRNA levels of beige cell markers (*Cd137*, *Tbx1*), mitochondria genes (*Cpt1a*, *Cpt2*), and lipolysis enzymes (*Atgl*, *Hsl*) were all considerably higher in *aNotch1* than in WT IngWAT (Fig. 1f). Similar browning phenotypes were observed in visceral EpiWAT, but not in BAT of the *aNotch1* mutant mice (Supplementary Fig. 2f–h).

In parallel we generated another mouse model, *aP2-Cre/Rbpj*$^{flox/flox}$ (*aRbpj*). Genotyping and quantitative PCR (qPCR) confirmed the deletion of *Rbpj* DNA and the lower expression levels of *Rbpj* mRNA in *aRbpj* adipose tissues than in WT counterparts (Supplementary Fig. 2d,i). Again, browner appearance of IngWAT was observed in *aRbpj* when compared with WT mice (Fig. 1g), associated with higher levels of BAT-specific genes (Fig. 1h). However, expression of these genes were not altered in the BAT (Supplementary Fig. 2i). Of note, the *aNotch1* and *aRbpj* mice both had higher rectal temperatures than their WT siblings (Fig. 1i,j), indicating that the higher UCP1 levels result in elevated thermogenesis *in vivo*.

Improved glucose metabolism in Notch mutant mice

In rodents and humans, brown adipocytes are shown to improve glucose metabolism and insulin sensitivity[35,36]. To check whether browning of WAT in *aNotch1* mice elicits beneficial metabolic effects, we conducted intraperitoneal (IP) glucose- and insulin-tolerance tests (GTT and ITT, respectively). Compared to their WT siblings, the *aNotch1* mice had lower blood glucose concentrations after glucose or insulin injection (Fig. 2a,b). We further measured insulin-stimulated glucose uptake by IngWAT explants, and found that *aNotch1* IngWAT absorbed ~ 65% more glucose than their WT counterparts (Fig. 2c). Improved glucose tolerance and insulin-stimulated glucose clearance were also observed in the *aRbpj* mice (Fig. 2d,e). These *in vivo* and *ex vivo* experiments together suggest that the genetic disruption of Notch signaling in adipose tissue improves insulin sensitivity and blood glucose tolerance.

A physiological characteristic of beige cells is their highly active metabolism coupled to thermogenesis. We examined the metabolic rate of *aNotch1* mice using indirect calorimetry approach. The *aNotch1* mice had higher rates of oxygen (O_2) consumption and carbon dioxide (CO_2) production, and expended more energy than WT mice (Fig. 2f–h). To examine whether the metabolic changes are dependent on UCP1 function, mice were acclimated at thermoneutral condition (28.3 °C) for 3–5 weeks to block functional activation of UCP1. Notably, thermoneutrality abolished the beneficial metabolic phenotypes of the *aNotch1* mice observed at room temperature, but not UCP1 protein expression

(Supplementary Fig. 3). This result suggests that browning of WAT in the *aNotch1* mice leads to UCP1-dependent improvements of energy expenditure.

Contrary to thermoneutrality, cold stress induces formation of beige adipocytes and their adaptive thermogenesis through UCP1 upregulation and sympathetic nerve stimulation[37]. Notably, IngWAT of *aNotch1* mice contained many more clusters of $UCP1^+$ cells than the WT counterparts after exposed to 4 °C for 1 week (Fig. 2i). In addition, adipocytes in the *aNotch1* IngWAT are predominantly multilocular and $UCP1^+$, whereas WT IngWAT only contain a small fraction of such cells (Fig. 2i). These morphological changes were associated with elevated expression of UCP1 and PGC1-α in cold-acclimated *aNotch1* compared to WT IngWAT (Fig. 2j). These results indicate that *aNotch1* mice are more adaptive to cold-induced thermogenesis.

The *aNotch1* mice were resistant to HFD-induced obesity

In light of their better glucose tolerance, insulin sensitivity and higher metabolic rate, we predicted that the *aNotch1* mice should be resistant to HFD-induced obesity. Indeed, the *aNotch1* mice were leaner after fed with HFD for 4 weeks (Fig. 3a), even though their daily energy intake was similar to that of the WT littermates (Fig. 3b). In addition, the *aNotch1* mice retained better glucose tolerance and higher insulin sensitivity after HFD feeding (Fig. 3c,d).

This observation prompted us to examine if HFD activates Notch signaling in WT mice. Upon HFD treatment, expression of *Lep*, a surrogate indicator of mature adipocytes and obesity, was increased by 20 folds (Fig. 3e), confirming the obesogenic effect of HFD. Coincidentally, mRNA and protein expression of Notch receptors and targets were induced by HFD (Fig. 3e,f). These results together suggest that activation of Notch signaling is associated with, and inactivation of Notch conversely prevents, HFD-induced obesity.

Adipocyte-specific activation of Notch signaling inhibits browning and glucose metabolism

As a complementary approach to the KO mouse models, we carried out gain-of-function studies using adiponectin *(Adipoq)-Cre*/*Rosa*^{N1ICD} mice (henceforth *Adipoq/N1ICD*). As expected, adipose tissue of *Adipoq/N1ICD* mice had higher expression levels of *N1ICD*, *Hes1* and *Hey1* (Fig. 4a). The *Adipoq/N1ICD* mice were slightly (~ 6%) heavier than their WT littermates even though they had similar food intake (Supplementary Fig. 4a,b). Notably, the *Adipoq/N1ICD* mice had lower glucose tolerance and insulin sensitivity compared with WT littermates (Fig. 4b,c). In addition, the metabolic rate and the body temperature of *Adipoq/N1ICD* mice were also lower (Fig. 4d–g), accompanied by lower expression levels of thermogenic and mitochondrial respiration-related genes in the IngWAT, but not in BAT (Fig. 4h,i). Furthermore, the *Adipoq/N1ICD* BAT accumulated more lipid droplets and the size of lipid droplets appeared larger than their WT counterparts (Fig. 4j). Compared to the WT mice, the *Adipoq/N1ICD* mice were also less responsive to cold-induced browning, manifested by lower abundance of $UCP1^+$ beige adipocytes and lower expression levels of UCP1 and PGC1-α proteins in IngWAT after acclimated to 4 °C

(Supplementary Fig. 4c,d). Thus, genetic activation of Notch signaling in adipocytes impairs body energy metabolism.

Notch signaling inhibits the expression of *Prdm16* and *Ppargc1a* in white adipocytes

To understand the cellular and molecular mechanisms through which Notch signaling regulates adipocytes, we first employed loss-of-function studies in cell culture. We cultured SVF preadipocytes from subcutaneous WAT of the *Notch1*$^{flox/flox}$ mice. Upon transfection with a Cre plasmid, the expression of *Notch1* and its downstream target *Hes1* were reduced by more than 50% (Fig. 5a), accompanied by an upregulation *Prdm16* and *Ppargc1a* expression (Fig. 5a). In parallel, we inhibited Notch signaling in WT white adipocytes with a γ-secretase inhibitor, DAPT. DAPT upregulated the expression of *Ucp1*, *Cidea*, *Prdm16*, and *Ppargc1a* genes (Fig. 5b and supplementary Fig. 5a,b). Similarly, adipocytes cultured from *aNotch1* IngWAT expressed higher levels of *Ucp1*, *Ppargc1a*, and *Prdm16* than the WT adipocytes (Supplementary Fig. 5c,d). Moreover, *aNotch1* inguinal adipocytes exhibited higher O_2 consumption rate (OCR) than WT adipocytes upon stimulation with palmitate (Supplementary Fig. 5e). These results demonstrate that inhibition of Notch signaling cell-autonomously enhances the expression of brown (beige) adipocyte-specific genes and cellular respiration of white adipocytes.

We also performed Notch gain-of-function studies using SVF cells isolated from the subcutaneous WAT of *Rosa*^{N1ICD} mouse, which overexpresses (OE) the constitutive active N1ICD upon Cre induction (Fig. 5c). Accordingly, *Prdm16* and *Ppargc1a* were inhibited by the N1ICD^{OE} (Fig. 5c). As N1ICD^{OE} upregulates *Hes1* and *Hey1*, we next investigated if OE of these genes are sufficient to mimic the observed effect of N1ICD^{OE}. Indeed, either Hes1^{OE} or Hey1^{OE} repressed the expression of *Prdm16* and *Ppargc1a* (Fig. 5d,e).

These results prompted us to ask whether the transcriptional repressor Hes1 can directly bind the promoter of *Prdm16* and *Ppargc1a*. Bioinformatics analysis identified consensus N-Box (CACNAG) sites in the proximal promoter regions of mouse and human *Prdm16* and *Ppargc1a* genes (Fig. 5f). Chromatin immunoprecipitation (ChIP) using a Hes1 antibody followed by qPCR assay using primers flanking the N-Box region showed that these predicted binding sites in *Prdm16* and *Ppargc1a* promoter regions were enriched by 3- and 13-fold, respectively (Fig. 5g). However, enrichment of these regions was abolished in *aNotch1* adipocytes (Fig. 5g). As a control, the Hes1 antibody failed to enrich random promoter regions that do not contain the N-Box sequence (Fig. 5g), confirming the specificity of Hes1 binding to N-Box. Furthermore, Hes1 inhibited *Ppargc1a* promoter-driven luciferase reporter activity (Fig. 5h). These results suggest that the canonical Notch target Hes1 can directly bind to the promoters of *Prdm16* and *Ppargc1a* to repress their expression, therefore inhibiting brown (beige) gene programs.

Notch inhibition induces browning and ameliorates obesity in *Lep*^{ob} mice

To explore the therapeutic potential of targeting Notch signaling to improve glucose metabolism, we treated WT mice with a pharmacological inhibitor of the Notch signaling. We injected littermate mice of similar body weight with dibenzazepine (DBZ), a γ-secretase inhibitor, or vehicle control for 5 days consecutively. Notably, DBZ-treated mice had better

glucose tolerance and insulin sensitivity than the control mice (Supplementary Fig. 6a,b). At the molecular level, DBZ treatment resulted in higher Ucp1 mRNA and protein expression in IngWAT and EpiWAT (Supplementary Fig. 6c,d). Adipocyte volume and number are positively correlated with leptin production[38], and we found that *Lep* expression and adiposity were reduced, but $UCP1^+$ adipocytes were increased after DBZ treatment (Supplementary Fig. 6e,f). Hence, Notch inhibition reduced adiposity and improved glucose homeostasis in healthy mice.

To further investigate if Notch inhibition ameliorates obesity under pathological conditions, we treated ob/ob mice deficient of *Lep* (Lep^{ob}) with DBZ. Mice were randomly grouped and showed no difference in body weight gain prior to treatment (Fig. 6a). Notably, DBZ treatment attenuated the body weight gain seen in the vehicle-treated control group, without affecting energy intake (Fig. 6a,b). The body weight differences were associated with reduced size and weight of various WAT depots in the DBZ-treated mice (Fig. 6c–e and Supplementary Fig. 7a,b). DBZ treatment also reduced liver weight and hepatic lipid accumulation (Fig. 6d and Supplementary Fig. 7a), consistent with previous observations that Notch promotes lipogenesis in hepatocytes and liver steatosis[39]. In addition, glucose tolerance and insulin sensitivity were improved by DBZ treatment (Fig. 6f). Consistent with reduced adiposity, DBZ treated mice showed a lower respiration exchange ratio compared with control mice (Fig. 6g), indicating that DBZ initiated a metabolic shift towards utilization of fat as the energy source. At the molecular level, DBZ inhibited the expression of Notch targets *Hes1*, *Hey1* and *Heyl* as well as *Lep* (Fig. 6h), but upregulated *Ucp1* and *Ppargc1a* expression (Fig. 6h). DBZ also suppressed expression of inflammatory cytokines *Cd68*, *Il6* and *Il1b* (Fig. 6i) that are associated with obesity in humans[40]. At end of the experiment, fed blood glucose concentrations remained low in the absence of DBZ injection (Fig. 6j), suggesting a long-term beneficial effect of adipose browning on glucose metabolism. These results altogether provide strong evidence that Notch signaling pathway can be pharmacologically targeted to prevent and treat obesity, and to improve glucose tolerance and insulin sensitivity.

DISCUSSION

Our study reveals a previously unrecognized yet critical role of Notch signaling in regulating the browning of adipose tissues and body insulin sensitivity. We have provided compelling genetic, physiological, metabolic, histological, cellular and molecular evidence to demonstrate that blockage of Notch signaling promotes browning of WAT. Conversely, activation of Notch signaling represses expression of genes critical for BAT biogenesis, and is associated with whitening of BAT and poor insulin sensitivity. As Notch signaling is highly conserved in the animal kingdom, we anticipate that our results in mice will be applicable to humans, though future studies dissecting the role of Notch signaling in human adipose tissues are imperative.

We used the *aP2-Cre* mice to drive deletion of *Notch1* or *Rbpj* in adipose tissues. Although the *aP2-Cre* expression domain falls predominantly in immature and mature adipocytes, leaky expression of this promoter was reported in several other cell types[41-44]. Coincidently, Notch inhibition has been shown to improve insulin sensitivity through regulating liver lipid

metabolism and attenuating atherosclerosis[45,46]. Even though we used a more adipocyte-restricted *Adipoq-Cre* mouse model[47] to show that Notch activation conversely induces whitening of BAT and reduces glucose tolerance, we cannot exclude the possibility that Notch signaling in other cell types may have also contributed the metabolic improvements of the *aNotch1* mice.

White to brown fat transition involves a series of cellular processes, including increased Ucp1 expression and mitochondria production, lipolysis, and β-oxidation. These features are all observed in the WAT but not BAT of Notch mutant mice. The differential responses of BAT and WAT to Notch signaling are perhaps due to the different embryonic origin of these tissues as well as cell type specific gene regulatory programs. Of note, the higher UCP1 level in *aNotch1* white adipocytes is associated with enhanced uncoupled respiration and thermogenesis, which may have led to a higher core body temperature. However, as mammalian body temperature is controlled by the central nervous system (CNS), the subtle increases in core body temperatures in the *Notch* mutants suggest that Notch signaling may also play a role in CNS-mediated body temperature regulation. Alternatively, as both Notch signaling and core body temperature exhibit circadian rhythms (i. e. oscillate during a day)[48,49], perturbations in Notch signaling may have altered the normal rhythm of core body temperature.

We used ChIP assay to demonstrate that the transcriptional co-repressor Hes1 directly binds to the promoter regions of *Ppargc1a* and *Prdm16*, whose expression are inhibited by Hes1 overexpression. Hey proteins can also inhibit expression of Hes1 targets through dimerization with Hes1[50]. Consistent with this notion, we observed that overexpression of Hey1 also inhibits the transcription of *Ppargc1a* and *Prdm16*. In addition, NICD may recruit GCN5, a cofactor of Rbpj transcription complex[51] and a major acetyltransferase of PGC1-α to repress its transcriptional activity[52]. Contradictory to our finding, Hes1 has been shown to positively regulate expression of Prdm16 during mouse neurogenesis[53]. As Hes1 is a canonical transcriptional repressor, it probably acts through other mediators to upregulate Prdm16 indirectly in the neural system. These observations underscore the significance of cell context-dependent action of Notch signaling[54].

We found that HFD increased Notch activity in WAT, and *aNotch1* mutants are resistant to HFD-induced obesity. These results indicate that activation of Notch signaling is linked to the initiation and development of obesity. Our observation is in agreement with a recent study showing that high-fat, high-cholesterol diet increased the expression of Dll4 (a Notch ligand) in atheroma and fat tissue in *LDLR*–deficient mice[46]. Currently it is unclear how Notch signaling is activated at onset of obesity. In addition, a recent study shows that excessive leptin production in diet-induced obesity mice activates Notch signaling in metastatic breast cancer cells[55]. As we observed that inhibition of Notch reduced expression of *Lep* in adipose tissues, it is possible that a positive feedback loop between Notch signaling and excessive leptin production together accelerates the development of obesity. Treating *Lep*^{ob} mice with γ-secretase inhibitor reduced body weight and ameliorated glucose metabolism, such drastic effect may be elicited not only by browning of white adipocyte, but also through targeting other important metabolic organs, including liver, intestine, which directly regulates lipid metabolism and nutrient absorption respectively[39,56].

Pharmacological approaches specifically targeting the adipose tissue will clarify the direct contribution of adipose tissue to metabolic improvements after Notch inhibition.

One important future question is whether Notch signaling is involved in the commitment and specification of progenitors to become beige versus classical white adipocytes. Several lines of evidence suggest that browning is an inherent capability restricted to certain cell population that has a standby or predisposed machinery to respond to browning cues[19,57]. As Notch signaling is widely employed to control cell fate during development, it is important to examine how Notch regulates the cell fate specification of embryonic beige progenitors.

ONLINE METHODS

Animals

All procedures involving mice were performed in accordance with Purdue University's Animal Care and Use Committee. The *Rbpj*$^{flox/flox}$ mouse was previously described[58] and kindly provided by Tasuku Honjo (Kyoto University). Other mice used were purchased from Jackson lab: *Notch1*$^{flox/flox}$ (Stock# 007181)[59], *aP2-Cre* (Stock# 005069)[60], *Adiponectin–Cre* (Stock# 010803)[47], *Lep*^{ob} (Stock# 000632)[61]. *Rosa*^{N1ICD} (Stock# 008159)[62], *Rosa*^{EYFP} (Stock# 007920). Mice were in C57BL/6J or mixed background and housed in the animal facility with free access to water and standard rodent chow food or high fat diet (TD.06414 Harlan). Energy intake assay was calculated by measuring food consumption and data was presented as the food weight multiple its energy content, then normalized to body weight of mice and # of days.

Indirect calorimetry study

Oxygen consumption (VO_2), carbon dioxide production (VCO_2), respiratory exchange ratio (VCO_2/VO_2) and heat production were measured using an indirect calorimetry system (Oxymax, Columbus Instruments) installed under a constant environmental temperature (22 °C) and 12:12 light cycle. Food and water were free access to mouse in each chamber.

Rectal temperature measurement

A digital thermometer (ETI model: MicroTherma 2) was used in combination with a copper thermocouple probe (Type T). The probe was inserted 2 centimeters and 1.6 centimeters into anal duct of male and female adult mice (2–4 month-old), respectively. Temperature was measured at around 4 pm.

Glucose uptake in WAT explants

Mice were fasted for 20 hours (from 6 pm to 2 pm of next day). Intact inguinal adipose tissue was carefully dissected free of visible connective tissue, and placed immediately in ice-cold PBS for 5 minutes. WAT explants were then transferred to 37 °C prewarmed DMEM (glucose free), supplemented with 10 nM insulin for 30 minutes at 37 °C with 5% CO_2. For glucose consumption measurement, WAT was then transferred to 24 wells with 1 ml DMEM supplemented with 100 nM insulin and 1,000 mg L^{-1} glucose per well, and incubated at 37 °C with 5% CO_2. Media (50 μl) were collected for glucose measurement at

60 and 120 minutes. Glucose consumption was calculated based on the glucose concentration of media collected and measured with glucose test strip (Accu-Check Active, Roche) read by a glucometer (Accu-Check Active, Roche).The readings were calibrated based on a standard curve plotted using a gradient of known concentrations of glucose in DMEM ($R^2 > 0.99$).

DBZ treatment

DBZ was purchased from TOCRIS Bioscience (Cat. No. 4489) and used following previous studies[45,63]. DBZ was dissolved in DMSO at 100 mM concentration. Upon use the stock was suspended at 1:100 dilution in a solution containing 0.5% Methocel E4M (w/v, Dow Chemical) and 0.1% Tween-80 (w/v Sigma) in H_2O. This working solution was mixed by vortex and sonication for 1 minute each, and IP injected at a dosage of 10 μmol DBZ per kg body weight. Control groups were injected with equal volumes of DMSO diluted in E4M/Tween-80 solution. Control and DBZ treatment groups were randomly grouped. To test the effect of DBZ on genetic induced obesity, ob/ob (*Lep*^{ob}) mice (6-week-old, male) were treated every other day for one month.

Blood glucose measurement

Five μl blood collected from tail vein was dropped onto glucose test strip (Accu-Check Active, Roche) and measured by a glucometer (Accu-Check Active, Roche). For glucose tolerance tests, mice were given intraperitoneal (IP) injection of 100 mg ml^{-1} D-glucose (2 g kg^{-1} body weight for standard diet fed, 1 g kg^{-1} for high fat diet fed and 0.5 g kg^{-1} for *Lep*^{ob} mice) after overnight fasting, and tail blood glucose concentrations were monitored. For insulin tolerance test, mice were fasted for 4 hours before IP administration of human insulin (Santa Cruz) (0.75 U kg^{-1} body weight) and tail blood glucose concentrations were monitored. For both GTT and ITT, mouse was singly caged with blinded cage number and random orders.

FACS and immunostaining

SVF cells were isolated from inguinal WAT of 2-month old wild-type mice that under chow diet. To examine subpopulations of macrophage cells in the SVF, cells were sorted based on CD11b and F4/80 staining of SVF cells. For immunostaining, the digested SVF cells were cultured overnight and attached cells were stained for CD68 (ab955).

Primary adipocyte culture, transfection and chemical treatment

Stromal-vascular fraction (SVF) cells were isolated from subcutaneous white adipose tissue unless otherwise stated. Adipose tissue was minced and digested with 1.5 mg mL^{-1} collagenase at 37 °C for 1.5 ~ 2 hours. The digestions were stopped with DMEM containing 10% FBS, filtered through 100 μm filters and centrifuged at 450 × g for 5 minutes. SVF cells were seeded and cultured in growth medium containing DMEM, 20% FBS, 1% penicillin/streptomycin at 37 °C with 5 % CO_2 for 3 days. Upon confluence, the cells were collected and electroporated using a Neon transfection system (Invitrogen). Briefly, 10^5 cells were suspended in 10ulelectroporation buffer, including 2.5 μg plasmids and electroporated (1,100 V, 10 ms, 3 times) using a 10 μl tip. After electroporation, the cells were seeded and

cultured in 6–well plates. All plasmids used were cloned as described[64]. Preadipocytes were induced to differentiate with induction medium contains DMEM, 10% FBS, 2.85 μM insulin, 0.3 μM dexamethasone (DEXA) (Sigma) and 0.63 mM 3-isobutyl-methylxanthine (IBMX) (Cayman Chemical) for 4 days, then 4 days in differentiation medium contains DMEM, 200 nM insulin and 10 nM T3 until adipocytes mature. During the induction and differentiation, cell was treated with 10 μM DAPT (N-[N-(3,5-difluorophenacetyl)-1-alanyl]-S-phenylglycine t-butyl ester) (Cayman Chemical).

Adipocyte oxygen consumption rate (OCR) measurement

Primary SVF cells from inguinal WAT were isolated and cultured for 3 days before plated in XF cell culture microplates (Seahorse Bioscience). SVF cells (10,000 cells) were seeded in each well and each sample has 8 replicates. After 6 days of differentiation, cultured adipocytes were washed twice and pre-incubated in XF medium for 1–2 h at room temperature. The oxygen consumption rate was measured by the XF extracellular flux analyzer (Seahorse Biosciences). The chemicals (final concentration, 0.2 mM Palmitate: 34 μM BSA, 2 μM Rotenone) were preloaded into cartridges and injected into XF wells in succession. OCR was calculated as a function of time (picomoles per minute).

Total RNA extraction, cDNA synthesis and real-time PCR

Total RNA was extracted from cells or tissues using Trizol Reagent according to the manufacturer's instructions. RNA was treated with RNase-free DNase l to remove contaminating genomic DNA. The purity and concentration of total RNA were determined by a spectrophotometer (Nanodrop 2000c, Thermo Fisher) at 260 nm and 280 nm. Ratios of absorption (260/280 nm) of all samples were between 1.8 and 2.0. Then 5 μg of total RNA were reverse transcribed using random primers with M-MLV reverse transcriptase (Invitrogen). Real-time PCR was carried out in a Roche Light Cycler 480 PCR System with SYBR Green Master Mix (Roche) and gene-specific primers as previously described[64,65]. The $2^{-\Delta\Delta Ct}$ method was used to analyze the relative changes in each gene's expression normalized against 18S rRNA expression.

Protein extraction and western blot analysis

Protein was isolated from cells or tissue using RIPA buffer contains 50 mM Tris-HCl (pH 8.0), 150 mM NaCl, 1% NP-40, 0.5% sodium deoxycholate and 0.1% SDS. Protein concentrations were determined using Pierce BCA Protein Assay Reagent (Pierce Biotechnology). Proteins were separated by sodium dodecyl sulfate polyacrylamide gel electrophoresis (SDS-PAGE), transferred to a polyvinylidene fluoride (PVDF) membrane (Millipore Corporation), blocking in 5% fat-free milk for 1 hour at room temperature, then incubated with primary antibodies in 5% milk overnight at 4 °C. The UCP1 (ab23841), N1ICD (ab8925) and Hes1 (ab71559) antibodies were from Abcam, and PGC1-α (sc-13067), GAPDH (sc-32233) and Actin (sc-130656) were from Santa Cruz Biotechnology. The horseradish peroxidase (HRP) conjugated secondary antibody (anti-rabbit IgG or anti-mouse IgG, Santa Cruz Biotechnology) was diluted at 1:5,000. Immunodetection was performed using enhanced chemiluminescence western blotting substrate (Pierce Biotechnology) and detected with a Gel Logic 2200 imaging system (Carestream). Alternatively, membrane was incubated with infrared secondary antibody

(Alexa Fluor 790 goat anti-mouse IgG, A11357, Alexa Fluor 680 goat anti-rabbit IgG, A21109, life technologies, USA) and the signals were detected by using the Odyssey infrared image scanning system. Results shown in figures are representative result from at least three independent experiments.

Hematoxylin-eosin (H&E) and immunohistochemistry (IHC) staining

Adipose tissues were fixed in 10% formalin for 24 hours at room temperature. Then the tissues were embedded into paraffin and cut at 4 μm thick, de-paraffinized, and rehydrated through xylene, ethanol, and water by standard methods. For antigen retrieval, slides were submerged in 0.01 M sodium citrate (pH 6.0) and heated to 96 °C for 20 minutes in a laboratory microwave (PELCO). Immunohistochemistry was performed on a Dako Autostainer (Dako, Carpinteria, CA). Slides were incubated with 3% hydrogen peroxide and 2.5% normal horse serum (S-2012, Vector), followed by incubation with rabbit polyclonal anti-UCP1 primary antibody diluted 1:200 in 2.5% normal horse serum (Vector, S-2012) for 60 minutes. Signal was detected with an anti-rabbit IgG Polymer Detection Kit (MP-7401, Vector) Labeling and was visualized with 3, 3′-diaminobenzidine (DAB) as the chromogen (SK-4105, Vector). Slides were counterstained with Harris hematoxylin (EK Industries, Joliet, IL) and whole slide digital images were collected at 20X magnification with an Aperio Scan Scope slide scanner (Aperio, Vista, CA). Images shown were representative result of at least three biological replicates. Scanned images of H&E staining were analyzed by Photoshop CS3 to calculate cell numbers. Averaged adipocyte size was calculated as the image area divided by cell numbers.

Chromatin immunoprecipitation (ChIP) and genomic DNA recombination assay

Cultured inguinal adipocyte of both wild-type and mutant mice was cross-linked with 1% formaldehyde in DMEM medium for 10 minutes at room temperature followed by the addition of 125 mM glycine for 5 min at room temperature, after which cells were washed 1 time with ice-cold PBS and scraped into SDS lysis buffer. The cells were further sonicated and diluted for immunoprecipitation with the indicated antibodies. The immunoprecipitates were eluted and reverse cross-linked overnight at 65 °C. DNA fragments were purified using the Cycle Pure kit (Omega Bio-Tek), and qPCR was performed with primers listed in Supplementary Table 1. Genomic DNA was extracted from adipose tissue and amplified with primers listed in supplementary Table 1.

Luciferase assay

HEK293A cells were seeded into 12–well plate 1 day before lipofectamine 2000 mediated transfection. PGC1-α promoter luciferase plasmid was purchased from Addgene, generated by Handschin C, et al[66]. For transfection of each well, 100 ng Renilla plasmid, 400 ng pGL3-Basic (or pGL3-PGC1-α) and 600 ng Hes1 plasmid (or its blank control plasmid) were cotransfected following manufacture’s instruction. Cells were harvested 36 hours after transfection and analyzed with Dual-Luciferase Reporter Assay System (Promega).

Statistical analyses

Trial experiments or experiments done previously were used to determine sample size with adequate statistical power. Measurement values that are beyond fence as determined by interquartile range were considered as outlier and excluded from following statistical analysis. All analyses were conducted with student *t* test with two-tail distribution. Comparison with a P value < 0.05 was considered significant.

Supplementary Material

Refer to Web version on PubMed Central for supplementary material.

ACKNOWLEDGEMENTS

We thank T. Honjo (Kyoto University, Japan) for providing the *Rbpj*$^{flox/flox}$ mice; Dow AgroScience for providing Methocel E4M reagent; K. Ajuwon for providing access to calorimetry facility; S. Koser and S. Donkin for assistance with luciferase assay; D. Zhou for Odyssey imaging facility support; T. Wiegand and C. Bain for assistance with histology; J. Wu and S. Hobaugh for maintaining mouse colonies; and members of the Kuang laboratory for comments. This work was partially supported by a grant from the US National Institutes of Health (R01AR060652).

References

1. Smith RE. Thermoregulatory and Adaptive Behavior of Brown Adipose Tissue. Science. 1964; 146:1686–1689. [PubMed: 14224520]
2. Nedergaard J, Cannon B. The changed metabolic world with human brown adipose tissue: therapeutic visions. Cell Metab. 2010; 11:268–272. [PubMed: 20374959]
3. Rosen ED, Spiegelman BM. Adipocytes as regulators of energy balance and glucose homeostasis. Nature. 2006; 444:847–853. [PubMed: 17167472]
4. Tran TT, Kahn CR. Transplantation of adipose tissue and stem cells: role in metabolism and disease. Nat Rev Endocrinol. 2010; 6:195–213. [PubMed: 20195269]
5. van Marken Lichtenbelt WD, et al. Cold-activated brown adipose tissue in healthy men. N Engl J Med. 2009; 360:1500–1508. [PubMed: 19357405]
6. Saito M, et al. High incidence of metabolically active brown adipose tissue in healthy adult humans: effects of cold exposure and adiposity. Diabetes. 2009; 58:1526–1531. [PubMed: 19401428]
7. Virtanen KA, et al. Functional brown adipose tissue in healthy adults. N Engl J Med. 2009; 360:1518–1525. [PubMed: 19357407]
8. Cypess AM, et al. Identification and importance of brown adipose tissue in adult humans. The New England journal of medicine. 2009; 360:1509–1517. [PubMed: 19357406]
9. Zingaretti MC, et al. The presence of UCP1 demonstrates that metabolically active adipose tissue in the neck of adult humans truly represents brown adipose tissue. FASEB J. 2009; 23:3113–3120. [PubMed: 19417078]
10. Cypess AM, et al. Anatomical localization, gene expression profiling and functional characterization of adult human neck brown fat. Nat Med. 2013; 19:635–639. [PubMed: 23603815]
11. Jespersen NZ, et al. A classical brown adipose tissue mRNA signature partly overlaps with brite in the supraclavicular region of adult humans. Cell Metab. 2013; 17:798–805. [PubMed: 23663743]
12. Lidell ME, et al. Evidence for two types of brown adipose tissue in humans. Nat Med. 2013; 19:631–634. [PubMed: 23603813]
13. Schulz TJ, et al. Brown-fat paucity due to impaired BMP signalling induces compensatory browning of white fat. Nature. 2013; 495:379–383. [PubMed: 23485971]
14. Fisher FM, et al. FGF21 regulates PGC-1alpha and browning of white adipose tissues in adaptive thermogenesis. Genes Dev. 2012; 26:271–281. [PubMed: 22302939]

15. Ohno H, Shinoda K, Spiegelman BM, Kajimura S. PPARgamma agonists induce a white-to-brown fat conversion through stabilization of PRDM16 protein. Cell Metab. 2012; 15:395–404. [PubMed: 22405074]
16. Seale P, et al. Prdm16 determines the thermogenic program of subcutaneous white adipose tissue in mice. J Clin Invest. 2011; 121:96–105. [PubMed: 21123942]
17. Frontini A, et al. White-to-brown transdifferentiation of omental adipocytes in patients affected by pheochromocytoma. Biochim Biophys Acta. 2013; 1831:950–959. [PubMed: 23454374]
18. Wu J, et al. Beige adipocytes are a distinct type of thermogenic fat cell in mouse and human. Cell. 2012; 150:366–376. [PubMed: 22796012]
19. Wang QA, Tao C, Gupta RK, Scherer PE. Tracking adipogenesis during white adipose tissue development, expansion and regeneration. Nat Med. 2013; 19:1338–1344. [PubMed: 23995282]
20. Rosenwald M, Perdikari A, Rulicke T, Wolfrum C. Bi-directional interconversion of brite and white adipocytes. Nature cell biology. 2013; 15:659–667. [PubMed: 23624403]
21. Ye L, et al. Fat cells directly sense temperature to activate thermogenesis. Proc Natl Acad Sci U S A. 2013; 110:12480–12485. [PubMed: 23818608]
22. Cao L, et al. White to Brown Fat Phenotypic Switch Induced by Genetic and Environmental Activation of a Hypothalamic-Adipocyte Axis. Cell Metabolism. 2011; 14:324–338. [PubMed: 21907139]
23. Shabalina IG, et al. UCP1 in Brite/Beige Adipose Tissue Mitochondria Is Functionally Thermogenic. Cell Rep. 2013; 5:1196–1203. [PubMed: 24290753]
24. Pfannenberg C, et al. Impact of age on the relationships of brown adipose tissue with sex and adiposity in humans. Diabetes. 2010; 59:1789–1793. [PubMed: 20357363]
25. Ouellet V, et al. Outdoor temperature, age, sex, body mass index, and diabetic status determine the prevalence, mass, and glucose-uptake activity of 18F-FDG-detected BAT in humans. J Clin Endocrinol Metab. 2011; 96:192–199. [PubMed: 20943785]
26. Schroeter EH, Kisslinger JA, Kopan R. Notch-1 signalling requires ligand-induced proteolytic release of intracellular domain. Nature. 1998; 393:382–386. [PubMed: 9620803]
27. Ross DA, Rao PK, Kadesch T. Dual roles for the Notch target gene Hes-1 in the differentiation of 3T3-L1 preadipocytes. Mol Cell Biol. 2004; 24:3505–3513. [PubMed: 15060169]
28. Garces C, et al. Notch-1 controls the expression of fatty acid-activated transcription factors and is required for adipogenesis. J Biol Chem. 1997; 272:29729–29734. [PubMed: 9368042]
29. Lai PY, Tsai CB, Tseng MJ. Active form Notch4 promotes the proliferation and differentiation of 3T3-L1 preadipocytes. Biochem Biophys Res Commun. 2013; 430:1132–1139. [PubMed: 23237809]
30. Urs S, et al. Effect of soluble Jagged1-mediated inhibition of Notch signaling on proliferation and differentiation of an adipocyte progenitor cell model. Adipocyte. 2012; 1:46–57. [PubMed: 23700510]
31. Vujovic S, Henderson SR, Flanagan AM, Clements MO. Inhibition of gamma-secretases alters both proliferation and differentiation of mesenchymal stem cells. Cell Proliferat. 2007; 40:185–195.
32. Osathanon T, Subbalekha K, Sastravaha P, Pavasant P. Notch signalling inhibits the adipogenic differentiation of single-cell-derived mesenchymal stem cell clones isolated from human adipose tissue. Cell Biol Int. 2012; 36:1161–1170. [PubMed: 22974058]
33. Huang Y, et al. gamma-secretase inhibitor induces adipogenesis of adipose-derived stem cells by regulation of Notch and PPAR-gamma. Cell Proliferat. 2010; 43:147–156.
34. Nichols AM, et al. Notch pathway is dispensable for adipocyte specification. Genesis. 2004; 40:40–44. [PubMed: 15354292]
35. Stanford KI, et al. Brown adipose tissue regulates glucose homeostasis and insulin sensitivity. J Clin Invest. 2013; 123:215–223. [PubMed: 23221344]
36. Orava J, et al. Different metabolic responses of human brown adipose tissue to activation by cold and insulin. Cell Metab. 2011; 14:272–279. [PubMed: 21803297]
37. Cannon B, Nedergaard J. Nonshivering thermogenesis and its adequate measurement in metabolic studies. Journal of Experimental Biology. 2011; 214:242–253. [PubMed: 21177944]

38. Rosenbaum M, Leibel RL. The role of leptin in human physiology. N Engl J Med. 1999; 341:913–915. [PubMed: 10486426]
39. Pajvani UB, et al. Inhibition of Notch uncouples Akt activation from hepatic lipid accumulation by decreasing mTorc1 stability. Nat Med. 2013; 19:1054–1060. [PubMed: 23832089]
40. Weisberg SP, et al. Obesity is associated with macrophage accumulation in adipose tissue. J Clin Invest. 2003; 112:1796–1808. [PubMed: 14679176]
41. Martens K, Bottelbergs A, Baes M. Ectopic recombination in the central and peripheral nervous system by aP2/FABP4-Cre mice: implications for metabolism research. FEBS Lett. 2010; 584:1054–1058. [PubMed: 20138876]
42. Urs S, Harrington A, Liaw L, Small D. Selective expression of an aP2/Fatty Acid Binding Protein 4-Cre transgene in non-adipogenic tissues during embryonic development. Transgenic Res. 2006; 15:647–653. [PubMed: 16952017]
43. Mullican SE, et al. A novel adipose-specific gene deletion model demonstrates potential pitfalls of existing methods. Mol Endocrinol. 2013; 27:127–134. [PubMed: 23192980]
44. Lee KY, et al. Lessons on conditional gene targeting in mouse adipose tissue. Diabetes. 2013; 62:864–874. [PubMed: 23321074]
45. Pajvani UB, et al. Inhibition of Notch signaling ameliorates insulin resistance in a FoxO1-dependent manner. Nat Med. 2011; 17:961–967. [PubMed: 21804540]
46. Fukuda D, et al. Notch ligand delta-like 4 blockade attenuates atherosclerosis and metabolic disorders. Proc Natl Acad Sci U S A. 2012; 109:E1868–1877. [PubMed: 22699504]
47. Eguchi J, et al. Transcriptional control of adipose lipid handling by IRF4. Cell Metab. 2011; 13:249–259. [PubMed: 21356515]
48. Gerhart-Hines Z, et al. The nuclear receptor Rev-erbalpha controls circadian thermogenic plasticity. Nature. 2013; 503:410–413. [PubMed: 24162845]
49. Bray SJ. Notch signalling: a simple pathway becomes complex. Nat Rev Mol Cell Biol. 2006; 7:678–689. [PubMed: 16921404]
50. Iso T, et al. HERP, a novel heterodimer partner of HES/E(spl) in Notch signaling. Mol Cell Biol. 2001; 21:6080–6089. [PubMed: 11486045]
51. Kurooka K, Honjo T. Functional interaction between the mouse Notch1 intracellular region and histone acetyltransferases PCAF and GCN5. J Biol Chem. 2000; 275:17211–17220. [PubMed: 10747963]
52. Coste A, et al. The genetic ablation of SRC-3 protects against obesity and improves insulin sensitivity by reducing the acetylation of PGC-1{alpha}. Proc Natl Acad Sci U S A. 2008; 105:17187–17192. [PubMed: 18957541]
53. Kinameri E, et al. Prdm proto-oncogene transcription factor family expression and interaction with the Notch-Hes pathway in mouse neurogenesis. PLoS One. 2008; 3:e3859. [PubMed: 19050759]
54. Schwanbeck R, Martini S, Bernoth K, Just U. The Notch signaling pathway: molecular basis of cell context dependency. Eur J Cell Biol. 2011; 90:572–581. [PubMed: 21126799]
55. Battle M, et al. Obesity induced a leptin-Notch signaling axis in breast cancer. Int J Cancer. 2014; 134:1605–1616. [PubMed: 24114531]
56. Zecchini V, Domaschenz R, Winton D, Jones P. Notch signaling regulates the differentiation of post-mitotic intestinal epithelial cells. Genes Dev. 2005; 19:1686–1691. [PubMed: 16024658]
57. Liu W, et al. A heterogeneous lineage origin underlies the phenotypic and molecular differences of white and beige adipocytes. Journal of cell science. 2013; 126:3527–3532. [PubMed: 23781029]
58. Han H, et al. Inducible gene knockout of transcription factor recombination signal binding protein-J reveals its essential role in T versus B lineage decision. Int Immunol. 2002; 14:637–645. [PubMed: 12039915]
59. Yang X, et al. Notch activation induces apoptosis in neural progenitor cells through a p53-dependent pathway. Dev Biol. 2004; 269:81–94. [PubMed: 15081359]
60. He WM, et al. Adipose-specific peroxisome proliferator-activated receptor gamma knockout causes insulin resistance in fat and liver but not in muscle. P Natl Acad Sci USA. 2003; 100:15712–15717.

61. Coleman DL, Hummel KP. The influence of genetic background on the expression of the obese (Ob) gene in the mouse. Diabetologia. 1973; 9:287–293. [PubMed: 4588246]

62. Murtaugh LC, Stanger BZ, Kwan KM, Melton DA. Notch signaling controls multiple steps of pancreatic differentiation. Proc Natl Acad Sci U S A. 2003; 100:14920–14925. [PubMed: 14657333]

63. Milano J, et al. Modulation of notch processing by gamma-secretase inhibitors causes intestinal goblet cell metaplasia and induction of genes known to specify gut secretory lineage differentiation. Toxicol Sci. 2004; 82:341–358. [PubMed: 15319485]

64. Wen Y, et al. Constitutive Notch activation upregulates Pax7 and promotes the self-renewal of skeletal muscle satellite cells. Mol Cell Biol. 2012; 32:2300–2311. [PubMed: 22493066]

65. Shan T, Liang X, Bi P, Kuang S. Myostatin knockout drives browning of white adipose tissue through activating the AMPK-PGC1alpha-Fndc5 pathway in muscle. FASEB J. 2013; 27:1981–1989. [PubMed: 23362117]

66. Handschin C, Rhee J, Lin J, Tarr PT, Spiegelman BM. An autoregulatory loop controls peroxisome proliferator-activated receptor gamma coactivator 1alpha expression in muscle. Proc Natl Acad Sci U S A. 2003; 100:7111–7116. [PubMed: 12764228]

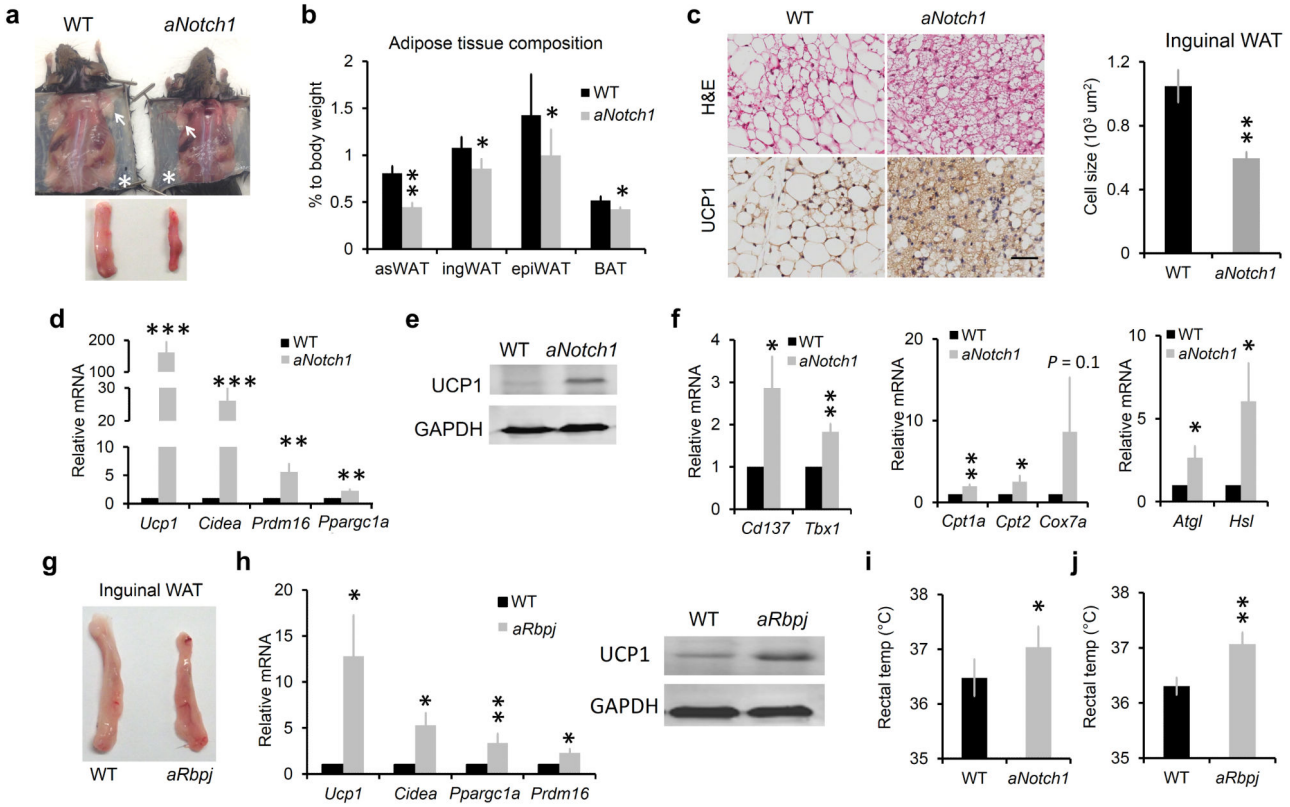

Figure 1.

Browning phenotype of WAT in *Notch* mutant mice. (**a**) Representative images of anterior-subcutaneous WAT (arrows) and IngWAT (asterisks), lower panel shows IngWAT. (**b**) Ratio of adipose tissue weight to body weight, $n = 7$ except for epiWAT ($n = 9$). (**c**) Representative images of Hematoxylin & Eosin (H&E) and UCP1 staining of IngWAT (left), scale bar, 50 μm, and average inguinal adipocyte size (right). (**d**–**f**) Relative expression of genes in WT and *aNotch1* IngWAT, (**f** middle, $n = 6$), (**f** right, $n = 8$). (**g**) Representative images of IngWAT from WT and *aRbpj* mice. (**h**) Gene expression in IngWAT. (**i**,**j**) Rectal temperature measurement, (**j**, $n = 7$). *$P < 0.05$, **$P < 0.01$, ***$P < 0.001$. Data are means ± SEM. $n = 4$ pairs of mice unless otherwise indicated.

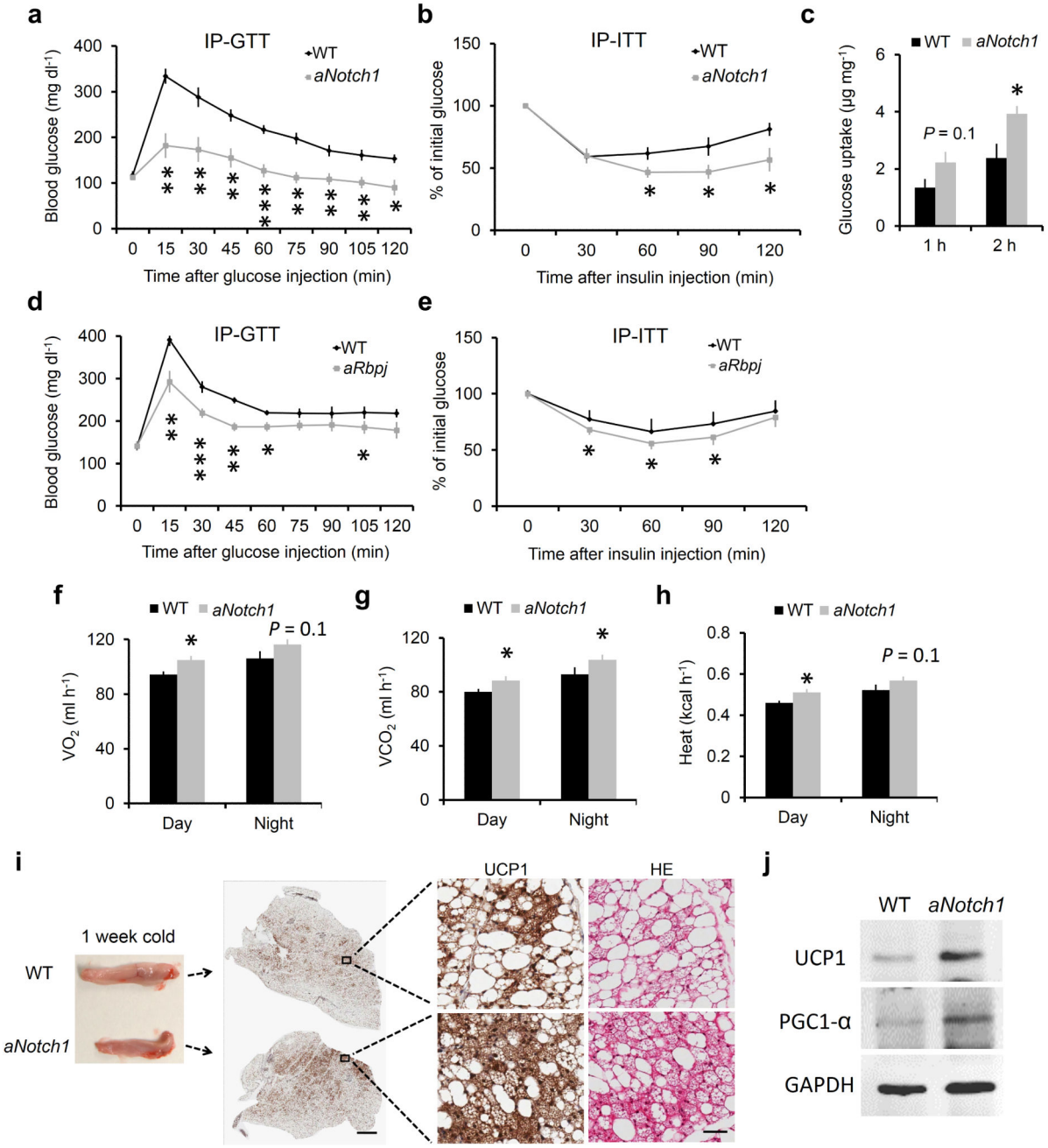

Figure 2.

Improved glucose metabolism in Notch mutant mice. (**a**,**b**) Blood glucose concentrations during IP-GTT (**a**) and IP-ITT (**b**) performed on 2–4 month-old WT and *aNotch1* mice, *n* = 6. (**c**) Insulin stimulated glucose uptake of IngWAT explant from fasted 2–4 month-old WT (*n* = 4) and *aNotch1* mice (*n* = 3). (**d**,**e**), IP-GTT (**d**, *n* = 4) and IP-ITT (**e**, *n* = 10) on 2–4 month-old WT and *aRbpj* mice. (**f–h**) Average day and night O_2 consumption, CO_2 production, and heat production, *n* = 6. (**i**) Representative histological analysis result of IngWAT from *aNotch1* and WT mice treated at 4 °C for 1 week, scale bar, 1 mm (middle),

50 μm (right). (**j**) Western blot result of sample as in panel **i**. **P* < 0.05, ***P* < 0.01, ****P* < 0.001. Data are means ± SEM.

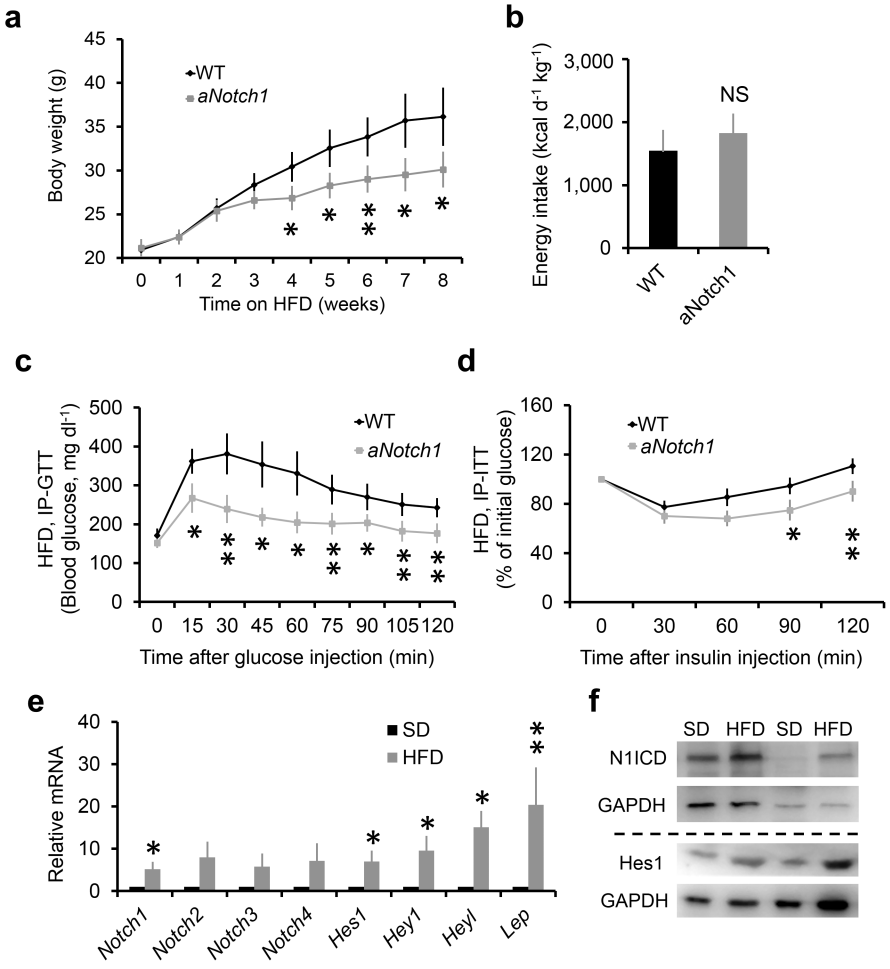

Figure 3.

aNotch1 mice were resistant to HFD-induced obesity. (**a**,**b**) Growth curve (**a**) and energy intake assay (**b**, $n = 4$) of WT and *aNotch1* fed with HFD. (**c**) Blood glucose concentrations during IP-GTT after glucose injection into fasted mice. (**d**) Blood glucose concentrations during IP-ITT after injecting insulin into fasted mice. (**e**) Gene expression assay of Notch receptors, Notch targets and *Lep* in WAT from 3 weeks' standard diet (SD) and HFD fed mice, $n = 8$. (**f**) Representative result of western blot for Notch activity of sample as in e. $^{*}P < 0.05$, $^{**}P < 0.01$, $^{***}P < 0.001$. Data are means ± SEM. $n = 5$ pairs of mice unless otherwise indicated.

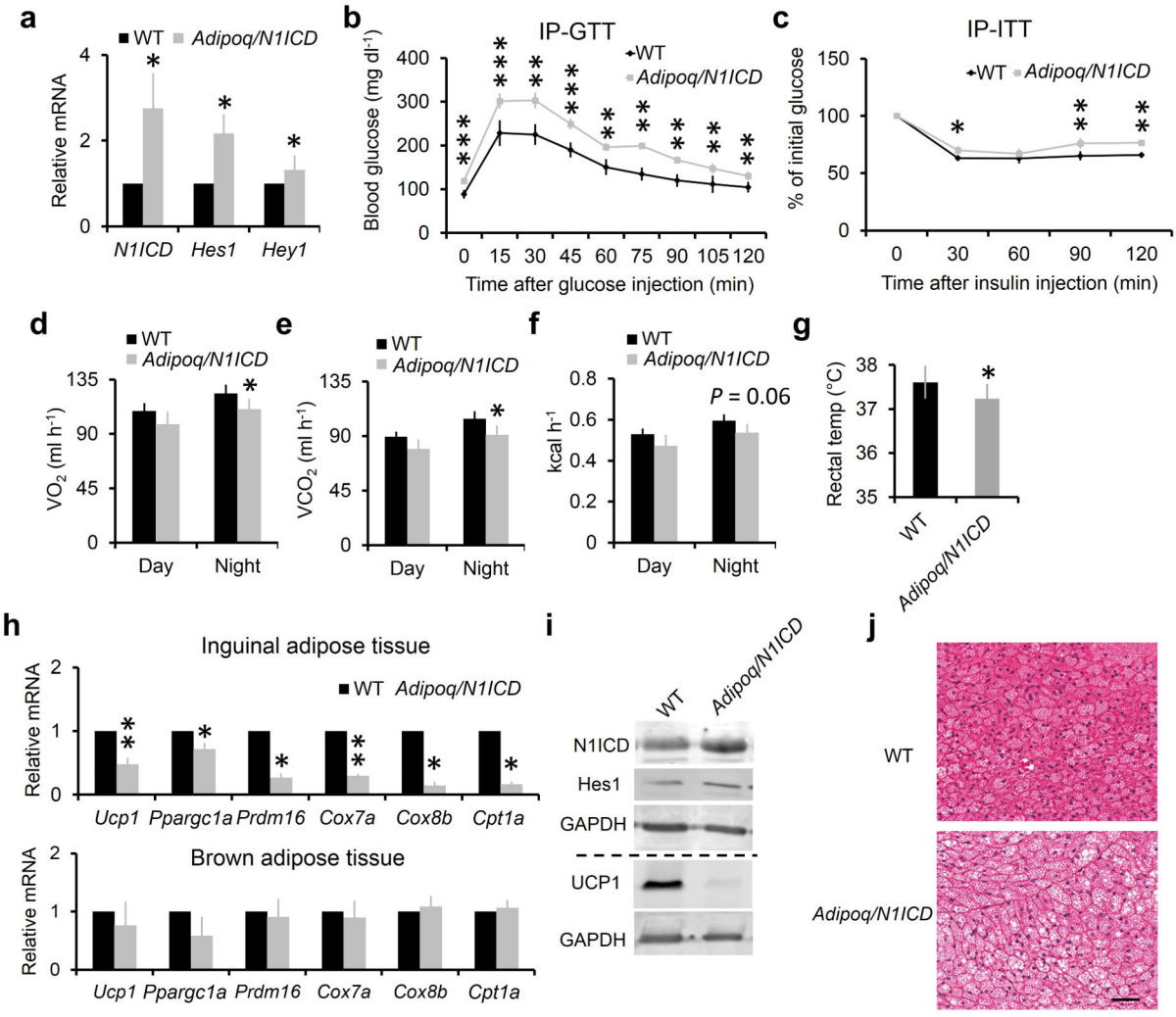

Figure 4.

Activation of Notch1 in adipocytes inhibits browning and glucose metabolism. (**a**) Relative expression of *N1ICD* and its target genes in WAT. (**b**,**c**) Blood glucose concentrations during IP-GTT (**b**, $n = 6$) and IP-ITT (**c**) performed on 5–8 week-old WT and A*dipoq/N1ICD* mice. (**d–f**) O_2 consumption (**d**), CO_2 production (**e**), and heat production (**f**). (**g**) Rectal temperature, $n = 5$. (**h**) Relative expression of BAT and mitochondria marker genes in IngWAT (top) and BAT (bottom). (**i**) Western blot of IngWAT. (**j**) H&E staining of BAT section, scale bar, 50 μm. $^{*}P < 0.05$, $^{**}P < 0.01$, $^{***}P < 0.001$. Data are means ± SEM. n = 4 pairs of mice unless otherwise indicated.

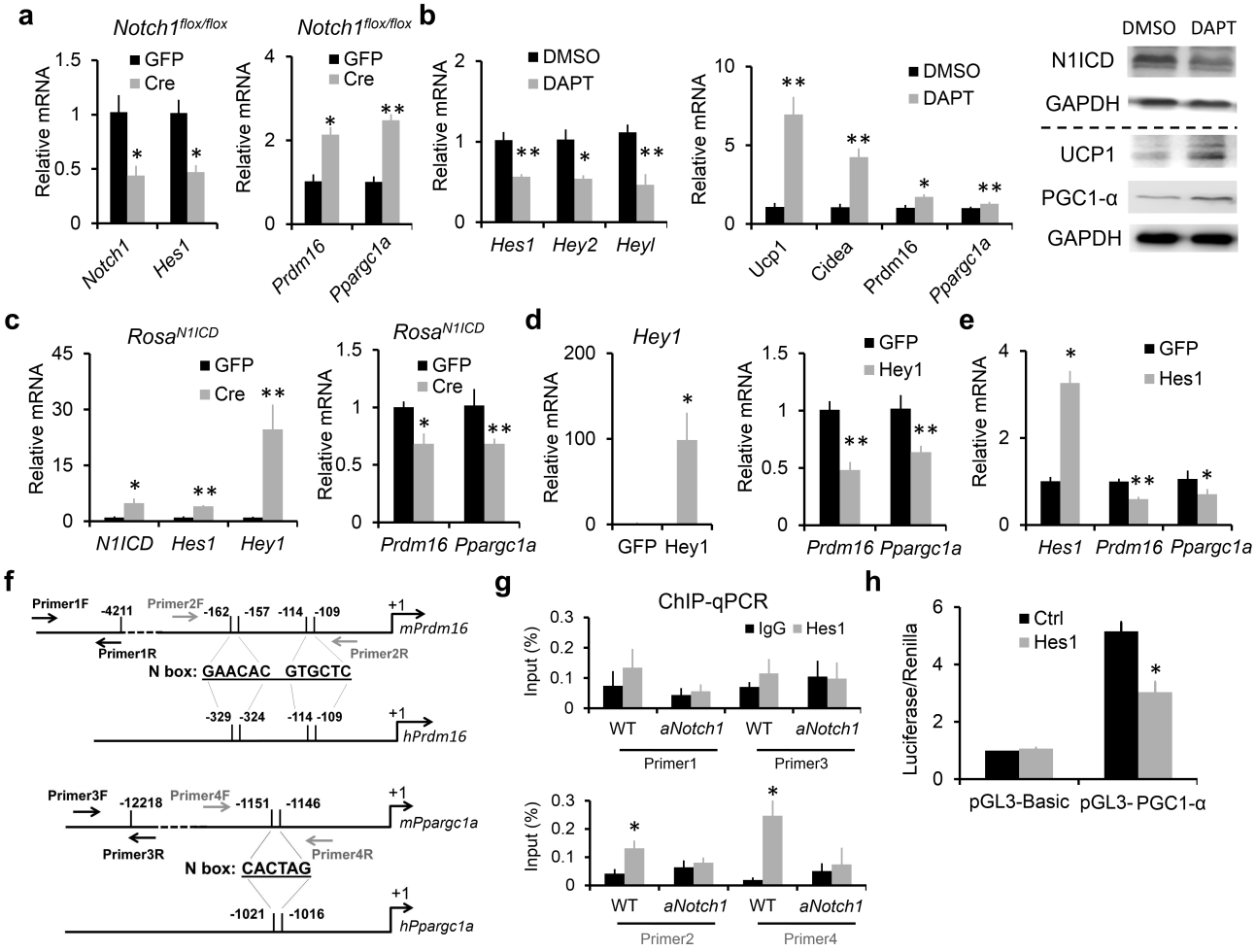

Figure 5.

Notch signaling inhibits expression of *Ppargc1a* and *Prdm16* genes in cultured white adipocyte. (**a**) Gene expression of *Notch1* and *Hes1* (left), *Prdm16* and *Ppargc1a* (right) in *Notch1*$^{flox/flox}$ preadipocytes after transfection with Cre or GFP plasmids (control). (**b**) Gene expression of Notch target (left), BAT-related genes (middle) and protein level of N1ICD, UCP1, PGC1-α (right) in cultured WT white adipocytes treated with DAPT during induction and differentiation, $n = 6$. (**c**) Gene expression in *Rosa*^{N1ICD} preadipocytes after transfection with Cre or GFP (control) plasmids. (**d**,**e**) Gene expression of WT preadipocytes after transfection with Hey1 (**d**) or Hes1 (**e**) plasmids. (**f**) Conserved N box domains on *Prdm16* (top) and *Ppargc1a* (bottom) promoters of both human and mouse. (**g**) Chromatin immunoprecipitation (ChIP) using Hes1 antibody followed by qPCR assay, $n = 4$. (**h**) Luciferase assay of HEK293 cells after cotransfection of pGL3-PGC1-α (or pGL3-Basic) plasmids with Renilla plasmids and Hes1 (or its control, ctrl) plasmids, $n = 5$. *$P < 0.05$ and **$P < 0.01$. Data are means ± SEM. $n = 3$ unless otherwise indicated.

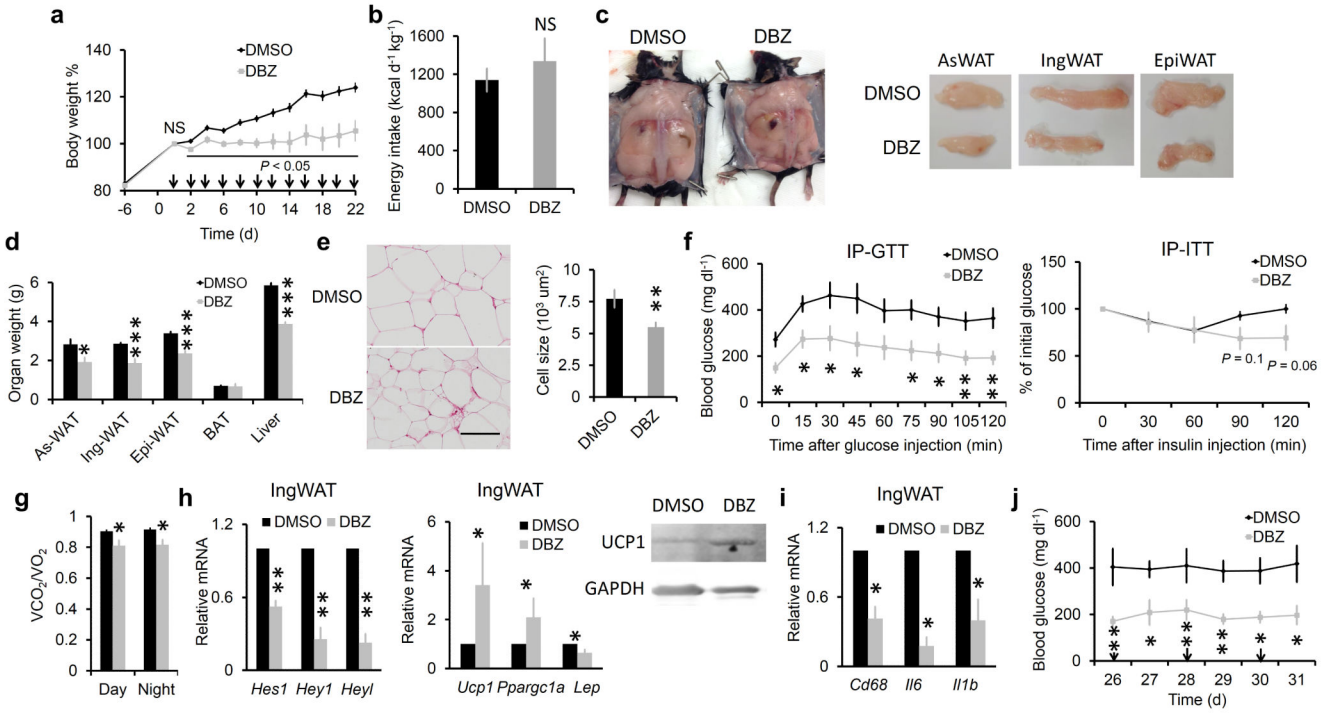

Figure 6.

Inhibition of Notch in *Lep* deficient obese mice (*Lep*^{ob}) ameliorates obesity and glucose metabolism. (**a**) Body weight ratio normalized to day 0, arrows mark doses of DMSO or DBZ injection. (**b**) Energy intake assay. (**c**) WAT images, anterior subcutaneous WAT (as-WAT). (**d**) Tissue weight. (**e**) H&E staining result of IngWAT, and adipocyte size. (**f**) Plasma glucose measurement during IP-GTT (left), or during IP-ITT (right). (**g**) Respiration exchange ratio of mice after treated with DMSO or DBZ for 22 days. (**h**,**i**), Relative expression of Notch targets (h left), adipocyte genes (**h** middle), UCP1 protein (**h** right), and inflammation-related genes (**i**) in IngWAT. (**j**) Fed-plasma glucose concentrations at dates shown, arrows indicate DMSO or DBZ injection (started from day 0 as shown in panel **a**). **P* < 0.05, ***P* < 0.01, ****P* < 0.001. Data are means ± SEM, *n* = 5.